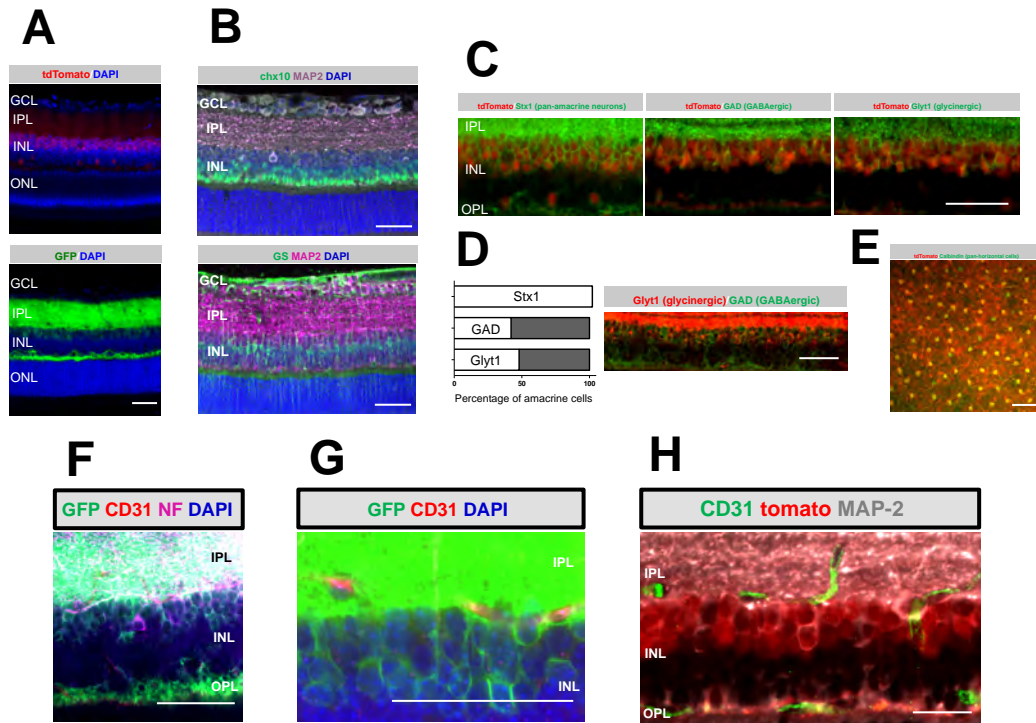


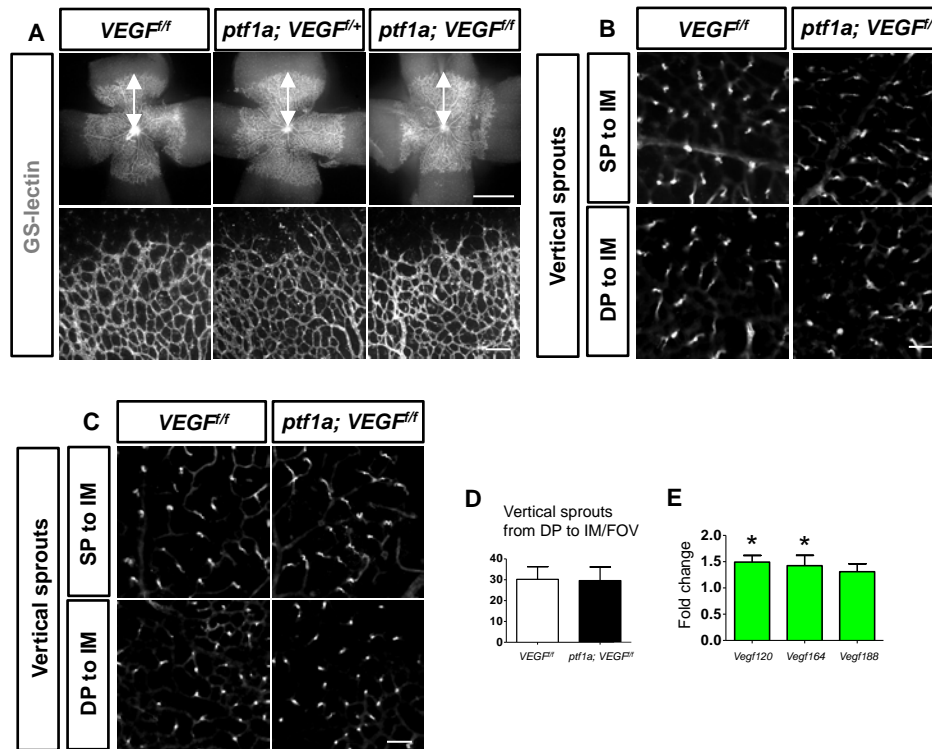
Supplemental Figure 1

Schematic diagram illustrating development of the vascular networks in the murine retina. The retinal vasculature forms as endothelial cells migrate from the optic nerve onto the retinal surface at birth and progress radially to form the superficial (or inner) plexus. Around postnatal day 7 (P7), sprouting vessels descend and advance into the OPL where they establish the deep plexus. At P11-12 stages, sprouting vessels from the deep plexus ascend into the IPL and ramify to form the intermediate plexus. GCL, ganglion cell layer; IPL, inner plexiform layer; INL, inner nuclear layer; OPL, outer plexiform layer; ONL, outer nuclear layer.



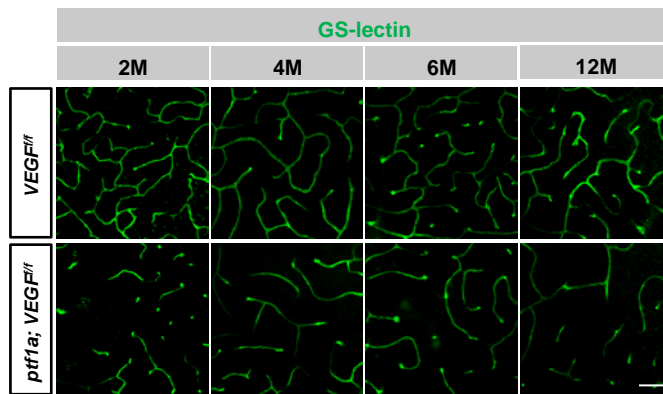
Supplemental Figure 2

Putative neurovascular units in the INL. **(A)** Whole retinal sections from mice harboring two Cre-recombination reporters and *ptf1a-Cre*. **(B)** IHC for bipolar (Chx10; top panel) and Mueller glia (glutamine synthetase (GS); bottom panel) is shown to highlight that their locations in the INL are distinct from amacrine cells. **(C)** Cre-mediated recombination occurs in amacrine cells in the inner margin of the INL and colocalizes with a pan-amacrine cell marker, Syntaxin 1 (Stx1), a GABAergic amacrine cell marker (GAD), and glycinergic amacrine cell marker (Glyt1) in cryosectioned retinas. **(D)** The percentage of Cre-positive amacrine cells that colocalized with amacrine cell subtypes was determined by counting cells in cryosectioned retinas (≥ 250 cells were counted for each cell type). **(E)** Colocalization of Cre-mediated recombination (td-Tomato) with calbindin positive horizontal cells at P23. **(F and G)** IHC on thick cut sections on *ptf1a-Cre;R26^{GFP/+}* mice with NF-M **(F)** and CD31 **(G)**. **(H)** Immunofluorescence for anti-MAP-2 and anti-CD31 in cryosections from P23 *ptf1a-Cre; R26^{tdTomato/+}* retinas. Scale bar: 50 μm **(A-G)**; 20 μm **(H)**. GCL, ganglion cell layer; IPL, inner plexiform layer; INL, inner nuclear layer; OPL, outer plexiform layer; ONL, outer nuclear layer.



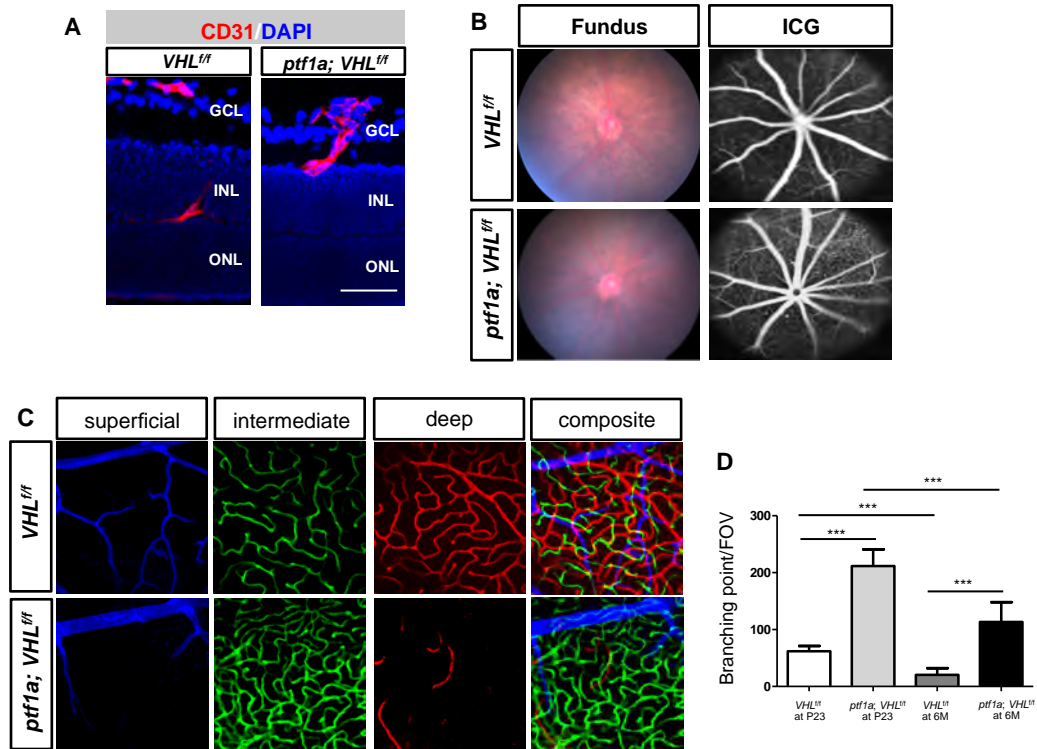
Supplemental Figure 3

The retinal vasculature of the superficial and deep plexuses are unaffected by *Vegfa* deletion in amacrine and horizontal cells. **(A)** Normal vascularization (bidirectional arrows) is observed in GS-lectin-positive P6 *ptf1a-Cre; VEGF^{f/f}* retinas and controls (*VEGF^{f/f}* (no Cre), *ptf1a-Cre; VEGF^{f/+}*). **(B-D)** Whole-mount staining in *VEGF^{f/f}* or *ptf1a-Cre; VEGF^{f/f}* retinas at P12 **(B)** or P15 **(C and D)**, reveals no differences in the number of vertical sprouts descending through the IPL from the superficial plexus or ascending through the INL from the deep plexus ($n = 4$). Scale bar: 1 mm **(A; upper panels)**; 100 μm **(A; lower panels)**; 50 μm **(B and C)**. **(E)** qPCR analysis showed that soluble VEGF120 and VEGF164 were the most abundant *Vegf* isoforms expressed in *ptf1a-Cre; VEGF^{f/f}* mice at P15 ($n = 4$). SP; superficial plexus, IM; intermediate plexus, DP; deep plexus.



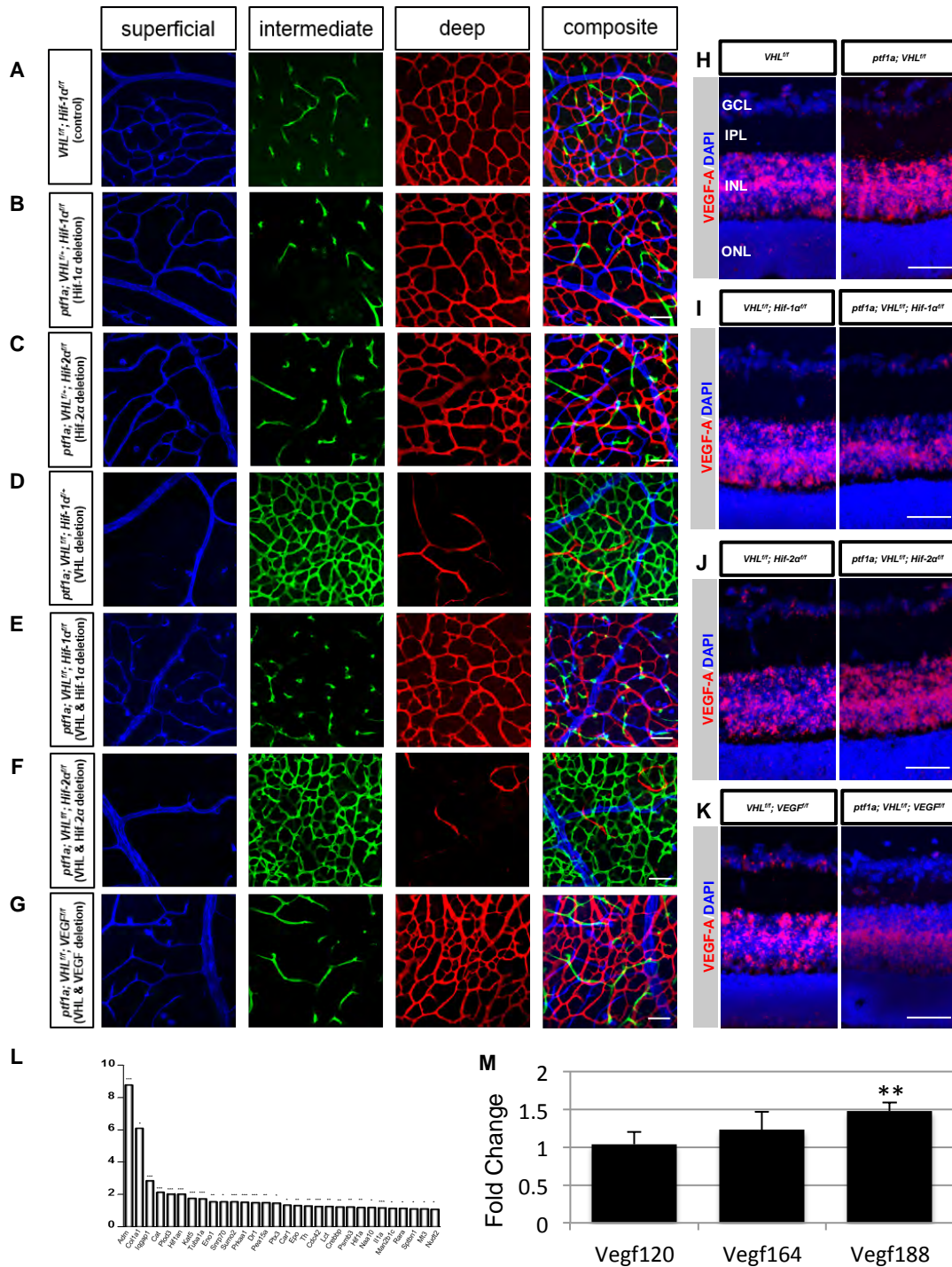
Supplemental Figure 4

Chronic intermediate plexus attenuation is observed in *ptf1a*-Cre; *VEGF* knockout mice. The intermediate plexus capillaries in the whole mount retinas of *VEGF*^{fl/fl} or *ptf1a*-Cre; *VEGF*^{fl/fl} mice at 2, 4, 6, 12 months. Scale bar: 50 μ m.



Supplemental Figure 5

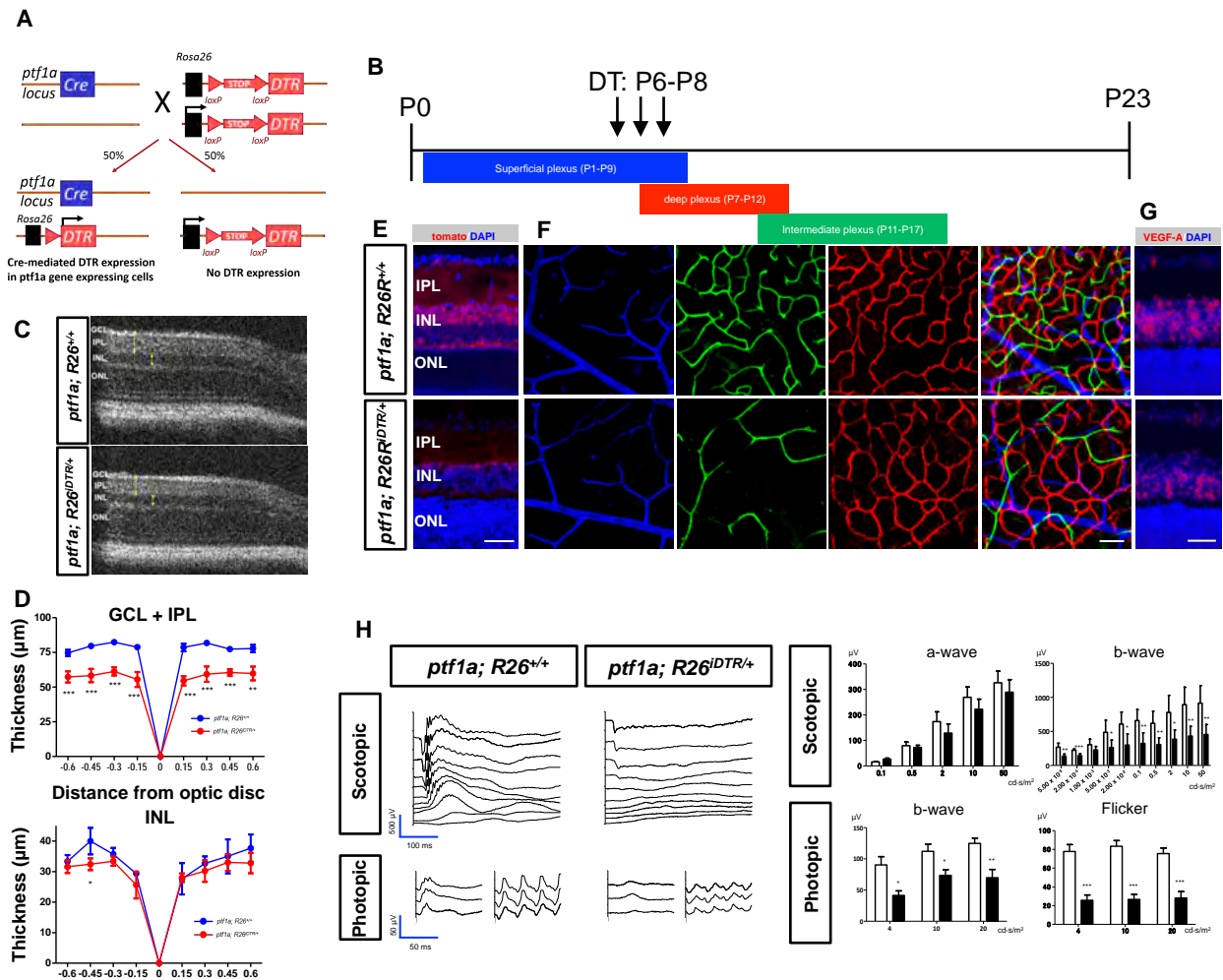
Blood vessels do not advance to the OPL in *Vhl* mutants (**A**) Vessels sprout from the superficial plexus towards the OPL in controls (*VHL^{f/f}* mice), but are directed towards the IPL in *ptf1a-Cre; VHL^{f/f}* mice at P5 where *Vegfa* is most highly expressed. (**B**) In vivo imaging of the ocular fundus and indocyanine green angiography in *ptf1a-Cre; VHL^{f/f}* mice and controls revealed dense vasculature. (**C** and **D**) The dense convoluted intermediate plexus, and attenuated superficial and deep plexuses persisted until as late as 20 months (**C**). Note that the abnormally high number of branching points persists in both groups longitudinally (**D**) ($n = 4-5$). *** $P < 0.001$; 2-tailed Student's *t* tests. Error bars indicate mean \pm SD. Scale bar: 50 μ m (**A** and **C**). GCL, ganglion cell layer; INL, inner nuclear layer; ONL, outer nuclear layer.



Supplemental Figure 6

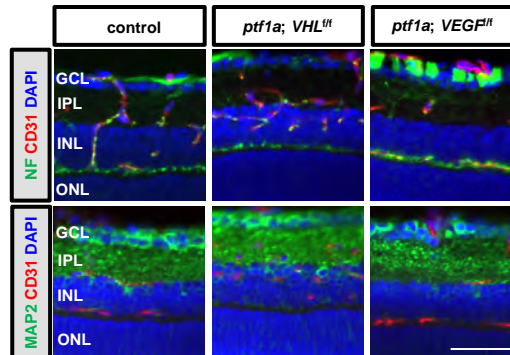
Early angiogenesis events (P12) are regulated by VHL/HIF-1α/VEGF signaling. (A-F) Combinatorial conditional knock-out strategies were employed to show that the loss of HIF-1α (B) but not HIF-2α (C) in amacrine and horizontal cells interferes with intermediate plexus development in haplosufficient *Vhl*^{+/-} mutants compared with controls (A). (D-F) Homozygous deletion of *Vhl* and *Hif-1α* (E) prevents the neovascularization observed in *Vhl* mutants, but deletion of HIF-2α elicits no effect (F) compared with controls (D). (G) Homozygous deletion of *Vhl* and *Vegfa* also rescues the *Vhl* phenotype. (H) *In situ* hybridization for *Vegfa* in *Vhl* mutants and controls. (I) *In situ* hybridization for *Vegfa* in double *Vhl*/*Hif-1α* mutants and controls. (J) *In situ* hybridization for *Vegfa* in double *Vhl*/*Hif-2α* mutants and controls. (K) *In situ* hybridization for *Vegfa* in double *Vhl*/*Vegfa* mutants and controls. (L) Relative mRNA expression values from qPCR gene-profiling analysis of 84 hypoxia signaling related genes in *ptf1a-Cre*; *VHL*^{fl/fl}; *VEGF*^{fl/fl} retinas at P12 compared with controls (harboring floxed alleles but no Cre); upregulated genes are plotted (*n* = 4). (M) Fold change of *Vegfa* isoforms in P12 *ptf1a-Cre*; *VHL*^{fl/fl}; *VEGF*^{fl/fl} retinas at P12 compared with controls. **P*<0.05, ***P*<0.01. ****P*<0.001; Scale bars: 50 μm (A-K).

Figure-S6 (Friedlander)



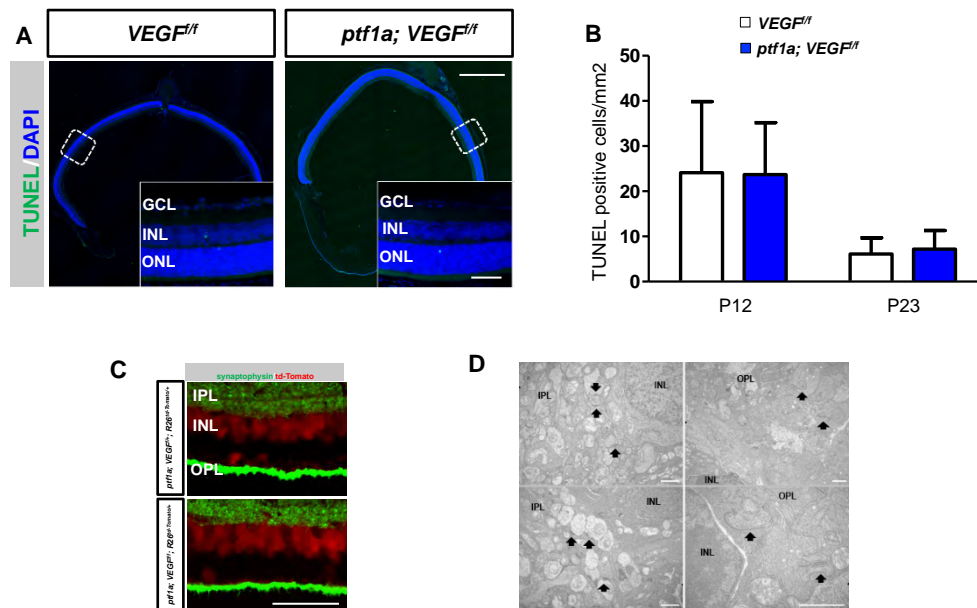
Supplemental Figure 7

The genetic ablation of amacrine and horizontal cells in mice results in attenuation of the intermediate plexus and negatively affects visual function. **(A)** Schematic of the experimental design for the genetic depletion of amacrine and horizontal cells in *ptf1a*-*Cre*; *R26*^{DTR/+} mice. **(B)** DT was injected daily from P6-8. **(C and D)** Thinning of the GCL/IPL and INL is observed *in vivo* using SD-OCT **(C)**, and quantified **(D)** in P23 *ptf1a*-*Cre*; *R26*^{+/+} and *ptf1a*-*Cre*; *R26*^{DTR/+} mice ($n = 6$). **(E)** IHC from P23 DT-treated *ptf1a*-*Cre*; *R26*^{DTR/+}; tdTomato/+ and *ptf1a*-*Cre*; *R26*^{+/+}; tdTomato/+ mice after DT treatment at P6-8 reveal a loss of the majority of amacrine and horizontal cells. **(F)** DT injections from P6-8 in P23 *ptf1a*-*Cre*; *R26*^{+/+} and *ptf1a*-*Cre*; *R26*^{DTR/+} staged mice induced attenuation of the intermediate plexus. **(G)** *in situ* hybridization was performed on P12 *ptf1a*-*Cre*; *R26*^{+/+} or *ptf1a*-*Cre*; *R26*^{DTR/+} retinas with a *Vegfa* probe and counterstained with DAPI. **(H)** Full-field ERGs performed on *ptf1a*-*Cre*; *R26*^{DTR/+} mice 3 months after DT treatment at P30-32 revealed reduced b waves and gross defects in cone-driven pathways ($n = 5-6$). * $P < 0.05$. ** $P < 0.01$. *** $P < 0.001$; 2-tailed Student's *t* tests. Error bars indicate mean \pm SD. Scale bar: 50 μm **(F, G)**; 40 μm **(E)**. GCL, ganglion cell layer; IPL, inner plexiform layer; INL, inner nuclear layer; ONL, outer nuclear layer.



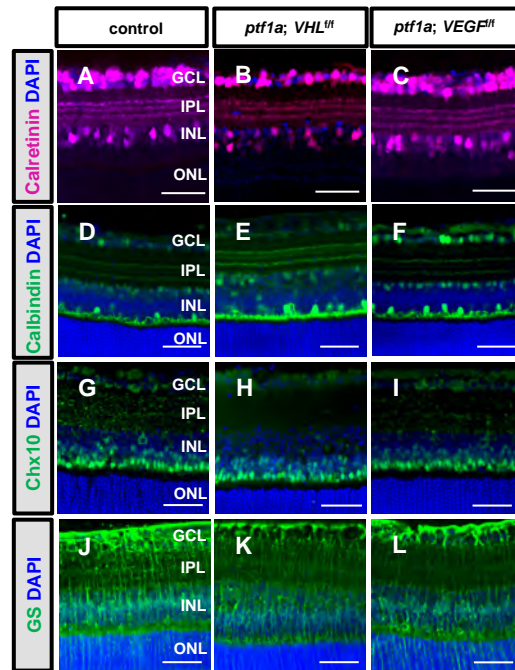
Supplemental Figure 9

Neurovascular units with the amacrine and horizontal cells and intraretinal capillaries in *ptf1a*-Cre; VEGF knockout and *ptf1a*-Cre; VHL knockout mice. Fluorescent immunostaining for anti neurofilament (NF) or anti-MAP2 with CD31 in retinal cryosections from P23 *ptf1a*-Cre; *VHL^{fl}* mice or *ptf1a*-Cre; *VEGF^{fl}* mice. The nuclei of cells were counterstained with DAPI (blue). Scale bar: 50 μ m. GCL, ganglion cell layer; IPL, inner plexiform layer; INL, inner nuclear layer; OPL, outer plexiform layer; ONL, outer nuclear layer.



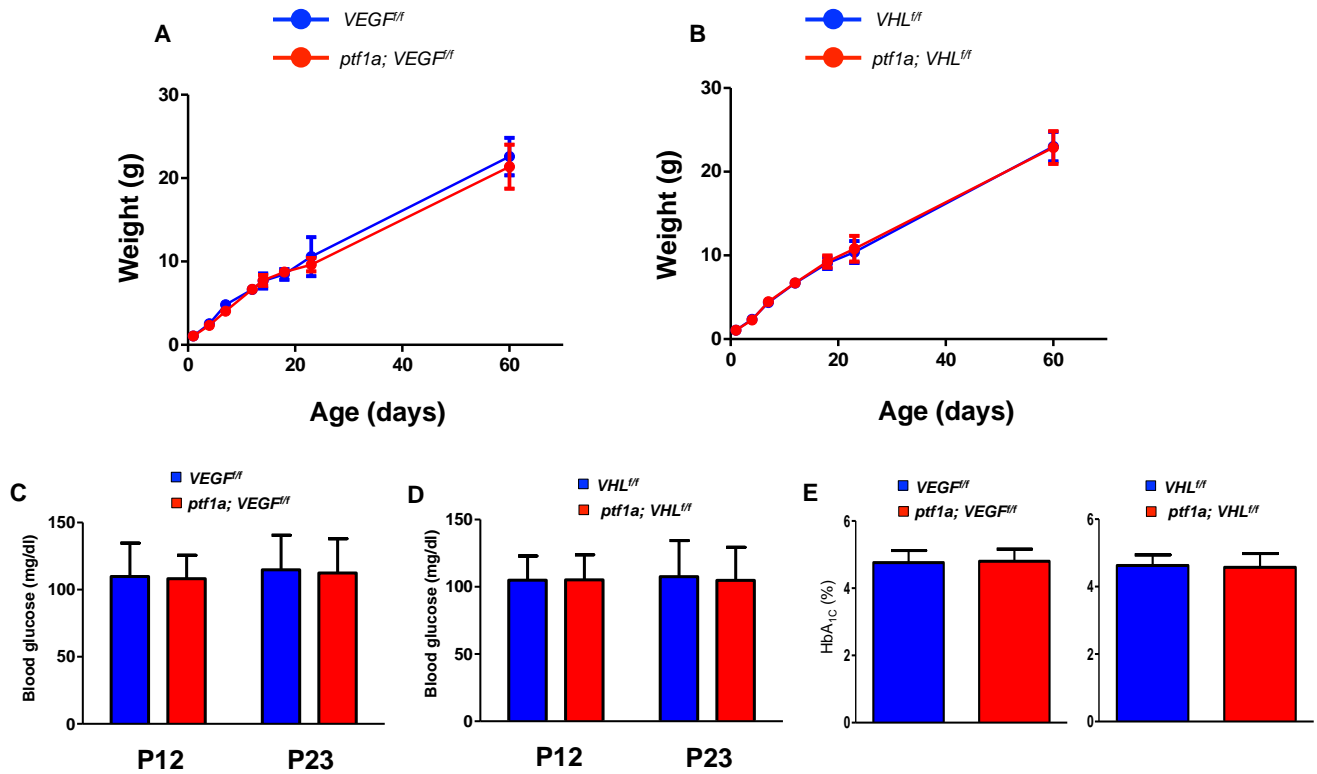
Supplemental Figure 10

No evidence of heightened neurodegeneration or abnormal synaptogenesis was observed in *ptf1a-Cre; VEGF^{f/f}* mice. **(A)** TUNEL staining of P12 *ptf1a-Cre; VEGF^{f/f}* retinas and controls. Scale bars: 500 μ m (**A**; upper right); 50 μ m (**A**; lower right). **(B)** Quantification from **(A)** at P12 or P23 ($n = 4$). **(C)** The expression pattern of synaptophysin is unremarkable in P15 *ptf1a-Cre; VEGF^{f/f}; R26^{tdTomato/+}* retinas. **(D)** Transmission electron micrograph showing normal synaptic ultrastructure (arrows) and synaptic vesicles in P23 *ptf1a-Cre; VEGF^{f/f}* retinas (upper panels: controls). Scale bar: 50 μ m (**C**); 1 μ m (**D**). GCL, ganglion cell layer; IPL, inner plexiform layer; INL, inner nuclear layer; ONL, outer nuclear layer; OPL, outer plexiform layer.



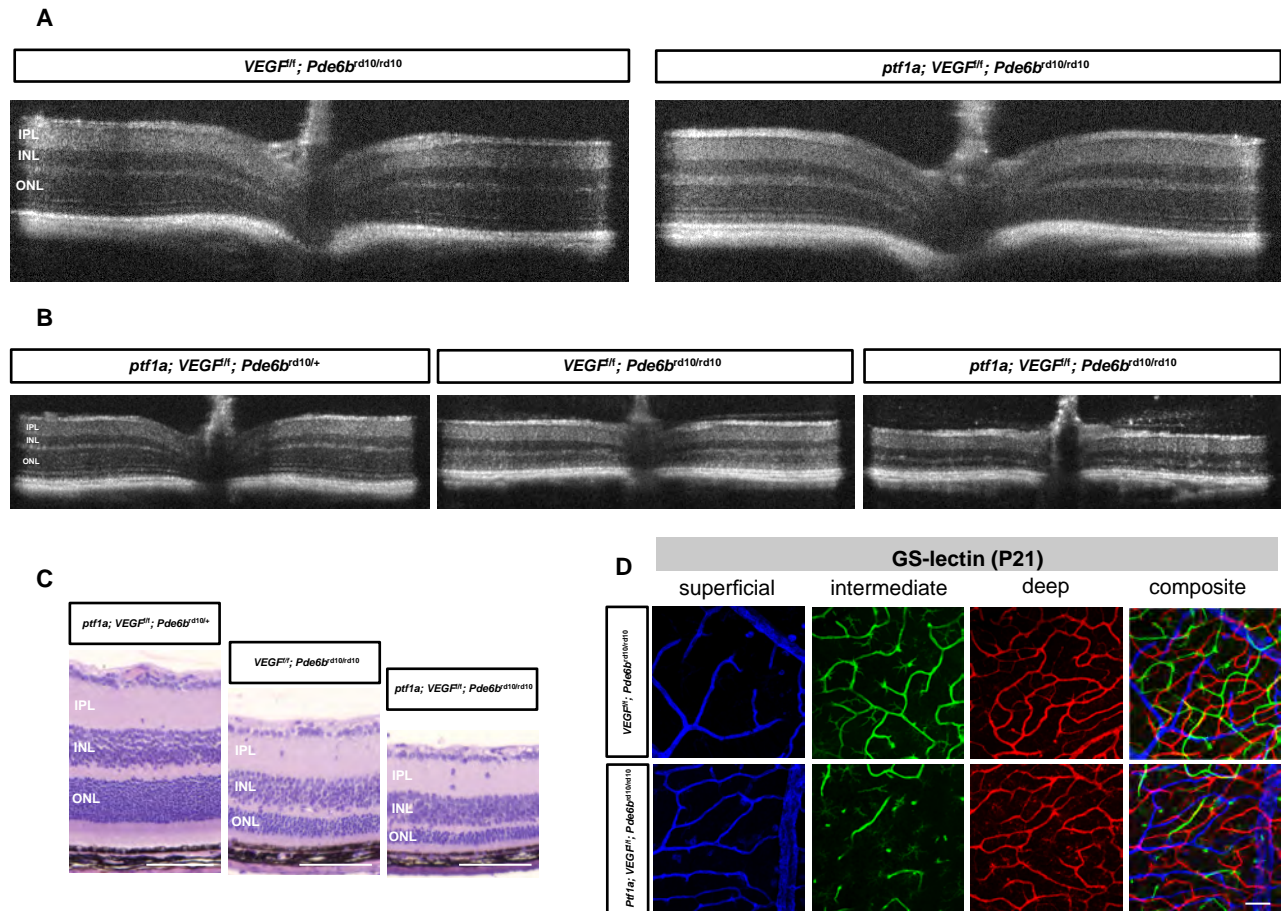
Supplemental Figure 11

No differences in the topographies of interneurons and Mueller glia are observed in *ptf1a*-Cre VEGF knockout and *ptf1a*-Cre; VHL knockout mice. (A-L) Cryosections from 23-day-old *ptf1a*-Cre; *VEGF^{fl}* and *ptf1a*-Cre; *VHL^{fl}* mice and controls were stained for calretinin (A-C), calbindin (D-F), chx10 (G-I), and glycogen synthase (GS) (J-L). The nuclei of cells were counterstained with DAPI (blue). Scale bar: 50 μ m in A-L GCL, ganglion cell layer; IPL, inner plexiform layer; INL, inner nuclear layer; ONL, outer nuclear layer.



Supplemental Figure 12

Normal weight, blood glucose, and HbA_{1c} levels in VEGF and VHL mutant mice. (A, B) Body weights in both groups were comparable. (*n* = 9-10). (C, D) Blood glucose was measured at P12 and P23 of *ptf1a-Cre; VEGF^{fl/fl}* mice and *ptf1a-Cre; VHL^{fl/fl}* mice. (*n* = 10 each). (E) HbA_{1c} levels in 4 month-old *ptf1a-Cre; VEGF^{fl/fl}* and 6 month-old *ptf1a-Cre; VHL^{fl/fl}* mice. (*n* = 8 each).



Supplemental Figure 13

Loss of VEGF in amacrine and horizontal cells accelerates photoreceptor atrophy in an animal model of retinal degeneration. **(A)** No degeneration (thinning of the ONL layer) is observed in SD-OCT images of P17 *ptf1a-Cre; VEGF^{fl/fl}; Pde6b^{rd10/rd10}* mice compared with controls (*VEGF^{fl/fl}; Pde6b^{rd10/rd10}*). **(B and C)** Significant ONL thinning is observed in rd10 mice with impaired intermediate plexuses (*ptf1a-Cre; VEGF^{fl/fl}; Pde6b^{rd10/rd10}*) compared with rd10 mice (*VEGF^{fl/fl}; Pde6b^{rd10/rd10}*), or with non-degenerating controls (one recessive *rd10* allele; *ptf1a-Cre; VEGF^{fl/fl}; Pde6b^{rd10/+}*) using OCT **(B)** and histology **(C)**. **(D)** The integrity of the intermediate plexus is shown in P21 *ptf1a-Cre; VEGF^{fl/fl}; Pde6b^{rd10/rd10}* mice (green) compared with controls (*VEGF^{fl/fl}; Pde6b^{rd10/rd10}*). Scale bar: 50 μ m **(C)**; 100 μ m **(D-F)**. IPL, inner plexiform layer; INL, inner nuclear layer; ONL, outer nuclear layer.